

See discussions, stats, and author profiles for this publication at: <https://www.researchgate.net/publication/51908049>

Adsorption of Nitric Oxide on Small Rh-n(+/-) Clusters: Role of the Local Atomic Environment on the Dissociation of the N-O Bond

ARTICLE in THE JOURNAL OF PHYSICAL CHEMISTRY A · DECEMBER 2011

Impact Factor: 2.69 · DOI: 10.1021/jp208847r · Source: PubMed

CITATIONS

3

READS

57

2 AUTHORS, INCLUDING:



R. A. Guirado-Lopez

Universidad Autónoma de San Luis Potosí

57 PUBLICATIONS 685 CITATIONS

SEE PROFILE

Adsorption of Nitric Oxide on Small Rh_n^{\pm} Clusters: Role of the Local Atomic Environment on the Dissociation of the N–O Bond

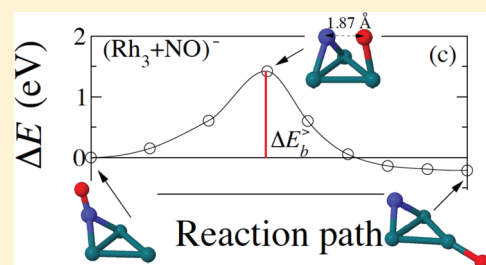
S. L. Romo-Ávila

Facultad de Ciencias, Universidad Autónoma de San Luis Potosí, Lateral Av. Salvador Nava s/n, 78290, San Luis Potosí, México

R. A. Guirado-López*

Instituto de Física “Manuel Sandoval Vallarta”, Universidad Autónoma de San Luis Potosí, Alvaro Obregón 64, 78000, San Luis Potosí, México

ABSTRACT: We present extensive pseudopotential density functional theory calculations dedicated to analyze the stability and dissociation behavior of NO molecules adsorbed on small nonmagnetic Rh_n^{\pm} clusters. Following the experimental work of Anderson et al. (*J. Phys. Chem. A* **2006**, *110*, 10992), we consider rhodium structures of different sizes ($n = 3, 4, 6$, and 13) and charge states onto which we attach NO species in both molecular and dissociative configurations. The relative stability between different Rh_n^{\pm} isomers depends on the ionization state of the clusters as well as on the presence of NO adsorbates on the surface. Various adsorbed configurations for the NO molecules are found when switching from cationic to neutral to anionic rhodium clusters. In particular adsorbed phases in which the NO molecule is attached with its N–O bond parallel to the plane of square or triangular facets are characterized by elongated nitrogen–oxygen interatomic distances, a fact that plays a fundamental role in the dissociation behavior of the adsorbate. We use the nudged elastic band method to analyze possible reaction pathways and transition states that could be present in our $(\text{Rh}_n + \text{NO})^{\pm}$ systems. We found (as in surface studies) that the dissociation of the N–O bond is more easily obtained on square facets than on triangular atomic environments, a fact that indirectly reveals the structure of Rh_n^{\pm} clusters present in the gas phase experiments. The energy barriers that need to be overcome to achieve the breaking of the N–O bond depend on the charge state of the systems, a result that could be used to tune the catalytic activity of these types of materials.



I. INTRODUCTION

Small clusters and nanoparticles have been extensively studied in the last years because they play, or promise to play, an important role in defining the properties of a wide range of systems, for example, in those where they are used as high-density recording materials,¹ as sensors,² in biomedical applications,³ as well as in catalytic devices.⁴ The last type of application is very interesting to study since it has been experimentally and theoretically demonstrated that the reactivity of clusters and nanoparticles is substantially modified by changing their size, structure, charge state, and chemical composition. For example, Burger et al.⁵ have revealed that small Au clusters efficiently catalyze the CO oxidation reaction at low temperatures. Hanmura and co-workers⁶ have demonstrated that the addition of hydrogen atoms to small Co cluster ions enhances the reactivity of the systems toward NO species while, in contrast, Swart and collaborators⁷ have found that the CO molecule dissociates on bare V clusters and it adsorbs intact on hydrogen-covered V_n systems. In the case of MoS_x ⁸ and V-doped Co_n ⁹ cluster alloys, the surface active sites strongly depend on the stoichiometry and chemical order within the particles, and finally, Anderson et al.¹⁰ as well as Ford and co-workers¹¹ have revealed the high activity of charged Rh_n^{\pm} clusters toward the dissociation of the NO molecule.

The experimental data obtained in refs 10 and 11 are important to emphasize since the catalytic removal of the NO

impurity from air is a relevant environmental problem. The decomposition of NO_x species on extended Rh surfaces has been extensively analyzed in the literature, and, clearly, the comparison of the data obtained in the small-cluster regime and the results found on surfaces can allow us to analyze to which extent changes in reactivity are caused by variations in the electronic structure or by local geometrical effects.

From surface studies it is well established that Rh is more efficient in the reduction of NO compared to Pd and Pt metals, but the reasons for the effectiveness of rhodium are still unclear. However, the role of the surface structure¹² [(111) or (100) termination], presence of steps,¹³ alloying effects,¹⁴ and the influence of oxygen preoccupation¹⁵ on the nitrogen oxide decomposition are well understood.

From the nanoparticle side, several studies have been reported addressing the adsorption properties and catalytic activity of single and bimetallic Rh-based nanoparticles deposited on various substrates. In particular, we mention the work of Nolte et al.,¹⁶ where they report global shape changes on Rh nanoparticles induced by the oxidation of its surface, together with the

Received: September 13, 2011

Revised: December 16, 2011

Published: December 22, 2011

paper by Grass and co-workers¹⁷ where they study the catalytic activity of the previous rhodium-oxide overlayer toward CO oxidation. Finally, in the report of Park and collaborators¹⁸ it is shown how it is possible to tune the catalytic CO oxidation rate by changing the composition of Rh–Pt bimetallic nanoparticles.

In the small-cluster regime, the reactivity studies performed by Anderson et al.¹⁰ and Ford and co-workers¹¹ on small gas phase $(\text{Rh}_n + \text{NO})^\pm$ complexes have revealed interesting trends. By using Fourier transform ion cyclotron resonance (FT-ICR) mass spectrometry, these authors have found, on the one hand, that cationic clusters react significantly faster than the anions, and, on the other hand, they propose that the nitric oxide decomposition process seems to be defined by a simple multistage mechanism. First, they assume that a dissociative chemisorption of the NO molecules on Rh_n^\pm occurs, generating N atoms that are highly mobile on the surface of the clusters. In a second step, these nitrogen atoms find each other and dimerize, and the as-formed N_2 molecules desorb from the surface. Finally, the O atoms remain on the Rh structure leading to the formation of a cluster oxide. The oxidation process continues until a limited oxygen coverage is achieved, after which NO is observed to molecularly adsorb on the oxidized Rh cluster without further N_2 evolution. The NO dissociation behavior discussed above has been formulated by only analyzing the mass spectra obtained after variable reaction times, but no direct information is available regarding the structure of the clusters or the adsorption state of N and O atoms.

From the theoretical side, the remarkable adsorption properties and catalytic activity of various types of Rh nanostructures have received a lot of attention. In particular, small clusters are very challenging due to their low symmetry, the presence of structural isomers, the possible existence of complex atomic relaxations, as well as finite size effects. In addition, small clusters, besides being more computationally tractable, better reflect the surface defects present in catalytic materials than do perfect extended surfaces, and, as a consequence, first principles theoretical studies are essential and need to be performed in order to shed some more light, at the molecular level, on the adsorption properties and catalytic activity of these types of materials.

In this respect, we would like to comment on the work of Harding et al.¹⁹ where they analyze, by using density functional theory (DFT), the structure, energetics, and reactivity of Rh_6 and Rh_6^+ clusters. They found that different Rh_6 clusters exhibit different reactivity toward NO molecules, a fact that could explain the different reaction kinetics experimentally observed by Ford et al.¹¹ for Rh clusters of this size. Their calculated energy barriers that need to be overcome in order to obtain the breaking of the N–O bond vary in the range of 0.23–1.62 eV, a result that reveals a complex interplay between reactivity and the electronic as well as geometrical characteristics of the underlying Rh clusters.

In this work, we have thus decided to perform a systematic DFT study dedicated to analyze the N–O bond dissociation behavior on small nonmagnetic Rh_n^\pm clusters. Following the experimental results of Anderson et al.,¹⁰ we consider different sizes ($n = 3, 4, 6$, and 13) and various cluster isomers to analyze the first step in the reaction, i.e., the adsorption and further dissociation of a single NO molecule. By using the nudged elastic band (NEB) method,²⁰ we study possible reaction pathways and transition states that could be present in our systems. By performing constrained and fully unconstrained structural optimizations, we will analyze the role of structural relaxation effects on the adsorption properties and catalytic activity. In addition to structure

and size aspects, we will also analyze the properties of cationic, neutral, and anionic Rh clusters. Our main goal will be thus to discuss the adsorption and dissociation of the NO molecule over a wide range of conditions in order to have a better understanding of the experimental data.

The rest of the paper is organized as follows. In section II we briefly describe the theoretical model used for the calculations. In section III we present our results analyzing the structural properties and the adsorption behavior, and finally, in section IV the summary and conclusions are given.

II. METHOD OF CALCULATION

The adsorption and dissociation behavior of NO molecules on small Rh_n^\pm clusters will be obtained within the density functional theory (DFT) approach using the ultrasoft pseudopotential approximation for the electron–ion interaction and a plane wave basis set for the wave functions as implemented in the PWscf code.²¹ For all our considered molecular structures, the cutoff energy for the plane wave expansion is taken to be 340 eV. A cubic supercell with a side dimension of 25 Å was employed in the calculations (which assures a negligible interaction between the images in our supercell approach) and the Γ point for the Brillouin zone integration. In all cases, we use the Perdew–Burke–Ernzerhof (PBE) pseudopotential²² including nonlinear core corrections and semicore state d in valence. We perform constrained and fully unconstrained structural optimizations using the conjugate gradient method. The convergence in energy was set as 1 meV, and the structural optimization was performed until a value of less than 1 meV/Å was achieved for the remaining forces on each atom.

To determine the minimum energy paths (in a static approximation) as well as the transition states, we applied the nudged elastic band (NEB) methodology.²⁰ The NEB calculation scheme is a chain-of-states method where a set of images between the initial and final states must be created to achieve a smooth curve. In our particular case, the relatively small size of our model cluster systems will ensure that the calculations for the reaction pathways will remain computationally tractable. In all our calculations, we use at least nine images to determine the energy profile, which have been found to be enough to clearly reveal the different stages of the NO dissociation reaction. The relevant energy barriers between well-defined reactants and products are obtained by calculating the energy difference of the initial position and the saddle point of each one of the energy profiles. Finally, we must comment that when analyzing cationic and anionic $(\text{Rh}_n + \text{NO})^\pm$ cluster complexes, the PWscf code includes a jellium background charge to maintain the charge neutrality, avoiding thus the well-known problem of divergence in the electrostatic energy.

III. RESULTS AND DISCUSSION

In this section we present our results addressing the stability and adsorption properties of $(\text{Rh}_n + \text{NO})^\pm$ molecular systems. All the calculations were nonmagnetic. This approximation could be justified since in the work of Harding et al.,¹⁹ in which they address the NO dissociation behavior on some Rh_6 isomers, variations of ~0.2 eV in the dissociation energy barriers are found for different spin multiplicities.

A. Energetics and Structural Properties of Bare Rh_n^\pm Clusters. We start our discussion by analyzing the properties of bare Rh_n^\pm clusters. We would like to comment first that spectroscopic investigations of small Rh clusters which can provide experimental details of their structure are limited. However, we

would like to particularly mention two papers recently published by Harding et al.²³ in which they combine far-infrared multiple photon dissociation spectroscopy and density functional theory calculations to investigate the geometrical structures of Rh_n^+ ($n = 6–12$) clusters. Based on a direct comparison between theory and experiments the authors conclude that (i) small Rh_n^+ clusters tend to favor structures based on octahedral and tetrahedral motifs and that (ii) the precise nature of the exchange-correlation functional plays (in most of the cases) a fundamental role in defining the energy ordering between different isomers. Actually, the previous finding was also theoretically suggested by Chou and co-workers.²⁴

Besides the above-mentioned problems related to differences in the calculations, there is also some degree of uncertainty in determining the actual cluster structures present in this kind of gas phase experiments due, on the one hand, to the always complicated problem of performing a complete search in multidimensional space and, on the other hand, because it is possible that different isomers could be favored by different charge states. Consequently, in this work, we do not intend to find global minimum atomic configurations. Instead, we will select a set of representative cluster structures to study the role of the cluster local atomic environment on the NO adsorption and dissociation of the N–O bond.

In Figure 1 we show the lowest energy atomic configurations for our considered neutral Rh_n clusters. For $n = 3$ and 4, we consider triangular (Figure 1a) and square (Figure 1b) atomic arrays, respectively, which are the fundamental units defining the (111) and (100) surfaces. For $n = 6$ we use two well-known isomers, namely, a trigonal prism (Figure 1c) and an octahedral configuration (Figure 1d). Finally, for $n = 13$ we consider an icosahedral cluster (Figure 1e) as well as two recently reported structures: a bilayer-like configuration (so-called BBP) found by Chang et al.²⁵ (Figure 1f) and a cubic structure reported by Bae and collaborators²⁶ (Figure 1g). From the optimized configurations we notice (as expected) that the nearest-neighbor interatomic distances in the clusters are considerably reduced (by up to 15%) when compared to the fcc Rh bulk value of 2.68 Å. This is due to the reduced coordination number of cluster atoms, this reduction being more notable in the smallest systems (see Figure 1a and b). In particular, the low-symmetry 13-atom clusters shown in Figure 1f and g are characterized by a complex distribution of Rh–Rh nearest-neighbor distances, ranging from 2.4 to 3.1 Å, a fact that will strongly influence the reactivity of the systems.

Within our pseudopotential approach we obtain that for Rh_6 the most stable structure (by ~ 0.25 eV) is the octahedral array (Figure 1d). In the case of the 13-atom isomers, the lowest energy atomic configuration corresponds to the bilayer-like cluster (Figure 1f); however, the cubic configuration (Figure 1g) is only located at 0.08 eV, the preferred isomer being more difficult to define. Finally, the icosahedral array (Figure 1e) is the less stable isomer by values as large as 1 eV.

Interestingly, we find that the extraction (Rh_n^+) or addition (Rh_n^-) of a single electron in our Rh clusters has a small effect on the bond lengths (which remained almost the same with variations as large as ± 0.1 Å) and on the global shape of the clusters. In contrast, notable perturbations in the energy differences between the various isomers are observed. For example for Rh_6 , when comparing the relative stability between the octahedral cluster and the trigonal prism, energy differences of $0.15 \rightarrow 0.25 \rightarrow 0.12$ eV are obtained when switching from cationic \rightarrow neutral \rightarrow anionic states, the most stable structure being always defined by the

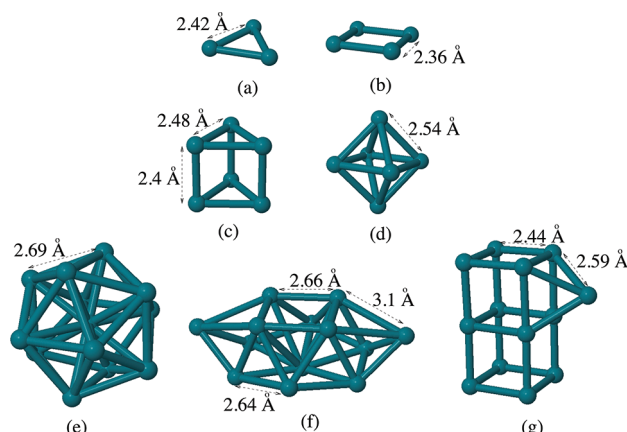


Figure 1. Calculated low-energy atomic configurations for neutral Rh_n clusters: (a) Rh_3 , (b) Rh_4 , (c) Rh_6 (trigonal prism), (d) Rh_6 (octahedral array), (e) Rh_{13} (icosahedra), (f) Rh_{13} (bilayer), and (g) Rh_{13} (cubic).

octahedral array (Figure 1d). In contrast, in the 13-atom case, the most stable Rh_{13}^+ structure is defined by the cubic configuration shown in Figure 1g, and finally, for the Rh_{13}^- cluster the bilayer-like structure is the most favorable (as in the neutral case), but with larger energy differences of 1.27 and 0.4 eV when compared to Figure 1e and g, respectively. These results imply that the stability of specific isomers in the samples could be altered by a charging mechanism, a fact that could modify the catalytic performance of cluster systems.

Finally, we expect that changing the charge state of Rh_n clusters will modify the location, orbital nature, and degeneracy of the highest occupied molecular orbital (HOMO) and lowest unoccupied molecular orbital (LUMO), as well as the energy level distribution around them, a fact that is also important to determine the adsorption properties. Actually, the relative position of the HOMO and LUMO levels of a given Rh_n cluster and a NO species is crucial since, following the ideas of the frontier orbital theory (FOT),²⁷ a small energy difference between $(\text{HOMO}_{\text{cluster}} - \text{LUMO}_{\text{NO}})$ or between $(\text{HOMO}_{\text{NO}} - \text{LUMO}_{\text{cluster}})$ will favor the existence of charge transfer and subsequent Rh–NO bond formation.

B. Energetics, Structural Properties, and Dissociation Behavior of $(\text{Rh}_n + \text{NO})^\pm$ Clusters. In the following sections, we present the energetics, structural properties, and dissociation behavior of several $(\text{Rh}_n + \text{NO})^\pm$ clusters. Clearly, there is a large number of adsorbed configurations that can occur on the surface of our considered Rh_n structures. However, following the work of Borg et al.²⁸ and Loffreda and co-workers¹² addressing the NO adsorption on extended Rh surfaces, we put special emphasis on the stability and dissociation behavior of the so-called lying-down chemisorbed array. In this case, the NO molecule is attached to Rh surfaces with the N–O bond parallel to the plane of square or triangular facets and defines a precursor state which is well-known to promote the easy dissociation of the NO molecule. The vertically adsorbed NO species with the N atom interacting with the surface has been found to be also highly stable, but, in this case, the rupture of the N–O bond requires first a reorientation process of the NO molecule to bring the O species in the vicinity of the surface. The previous molecular bending has been found to limit the N–O bond breakage since it involves high activation energies.

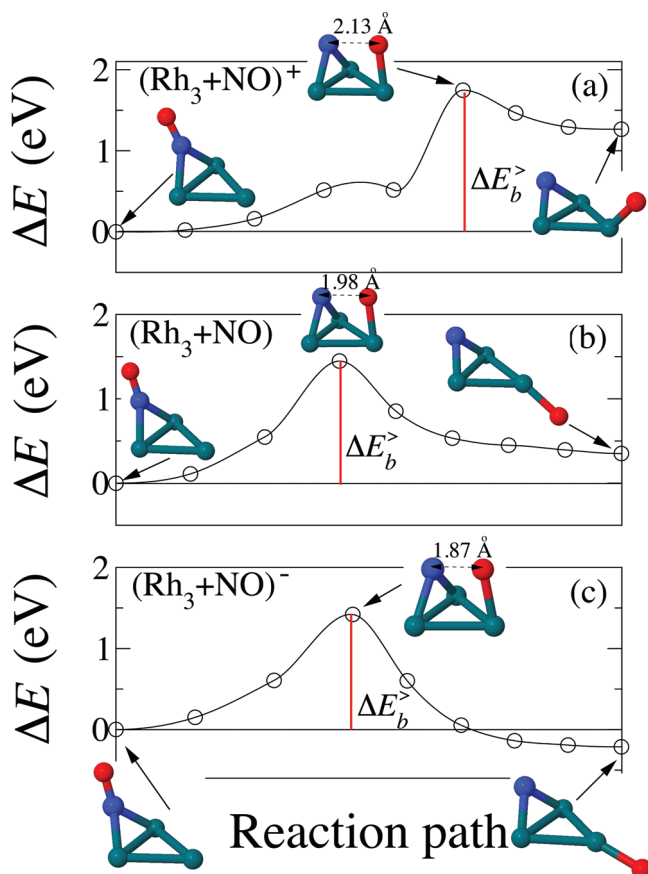


Figure 2. Calculated low-energy atomic configurations for $(\text{Rh}_3 + \text{NO})^\pm$ systems. In (a) and (b) we show results for molecular and dissociative NO adsorption, respectively. In (c) we show our data for the NO molecule attached in a lying-down array. In the left, middle, and right columns we show results for cationic, neutral, and anionic complexes, respectively.

In the case of dissociated arrays, we always consider chemisorbed O and N atoms located as close as possible to the vertical and lying-down molecular adsorptions. This is important in order to have reaction paths as free as possible from contributions arising from diffusion processes of N and O atoms, yielding thus our NEB data and more specific information about the breaking of the N–O bond. Clearly, finding the lowest energy atomic configuration of dissociated N and O atoms adsorbed on the surface of Rh clusters is a very complex issue. This has been clearly illustrated by Torres et al.²⁹ in a recently published paper in which they extensively analyze both molecular and dissociated chemisorption of NO species on two (neutral and positively charged) well-known Rh_6 isomers.

Finally, and unless otherwise specified, all the Rh atoms are constrained to reside at their equilibrium positions found in Figure 1, while the N and O species are allowed to relax freely. However, as will be discussed in the next sections, the role of cluster-relaxation effects on the NO adsorption and dissociation will be analyzed.

1. $(\text{Rh}_3 + \text{NO})^\pm$ Clusters. In Figure 2 we show, for different charge states, some low-energy atomic configurations for a NO molecule adsorbed in both molecular (Figure 2a and c) and dissociated (Figure 2b) configurations on the Rh_3 cluster shown in Figure 1a. From Figure 2a we see first that, for all the charge

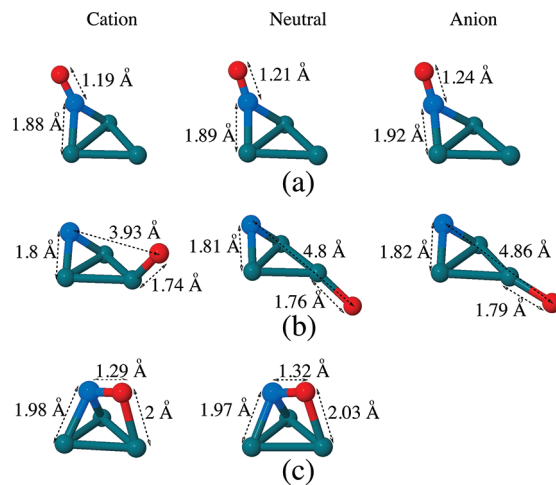


Figure 3. Reaction energy paths connecting the locally stable atomic configurations shown in Figure 2a-left, a-middle, and a-right with Figure 2b-left, b-middle, and b-right, respectively (shown as insets in the figures). In (a), (b), and (c) we show results for cationic, neutral, and anionic ($\text{Rh}_3 + \text{NO}$) systems, respectively. In the figure we also specify the values of the N–O interatomic separation at the transition state as well as the height of the direct dissociation energy barrier $\Delta E_b^>$ (see text).

states, the nitric oxide is stable as a vertically attached (on-bridge) chemisorbed species, characterized by $R_{\text{Rh}-\text{N}}$ and $R_{\text{N}-\text{O}}$ distances of ~ 1.9 and 1.2 Å, respectively. These values are close to those obtained in previous calculations^{12,13,15,30} addressing NO adsorption on extended (111) Rh surfaces. Next, in Figure 2b we plot low-energy atomic configurations for some possible dissociated arrays. Note that the chemisorbed N and O atoms, even if they are close to each other, do not recombine and are also stable as individual species on Rh_3^\pm . The N–O interatomic distance varies in the range of 3.9 – 4.8 Å, the largest values being found for the anionic cluster. In addition, almost equal $R_{\text{Rh}-\text{N}}$ and $R_{\text{Rh}-\text{O}}$ bond lengths are obtained for the different charge states, being in the range of 1.75 – 1.82 Å. Finally, we observe that in the positively charged and neutral species shown in Figure 2c-left and c-middle, respectively, the NO molecule can be stable in a horizontal lying-down geometry; however, the corresponding cluster anion is absent. The lying-down adsorbed phase is characterized by elongated N–O interatomic distance of ~ 1.3 Å, indicating the existence of a weakened bond relative to gaseous NO (1.17 Å). The previous activation of the N–O bond will be an important ingredient to more easily achieve the dissociation of the nitric oxide.

Concerning the relative stability between the different isomers, we would like to comment that, for cationic and neutral species, the vertically attached configuration (see Figure 2a-left and a-middle) is the most stable atomic array while, in the anionic state, the dissociated adsorbed phase (Figure 2b-right) is preferred. Finally, the lying-down adsorbed configuration is always the less stable structure by values as large as ~ 0.5 eV.

In Figure 3 we present the reaction paths calculated with the NEB methodology presented in section II. In Figure 3a, b, and c we plot the reaction energy paths linking Figure 2a-left, a-middle, and a-right with Figure 2b-left, b-middle, and b-right, respectively. We include as insets the initial and final atomic configurations, as well as the calculated transition state, located at the maximum of the energy paths. We see from the figures that, for the different charge states, NO dissociation in the triangular Rh_3 cluster involves high direct energy barriers $\Delta E_b^>$, ranging from 1.4 to 1.7 eV,

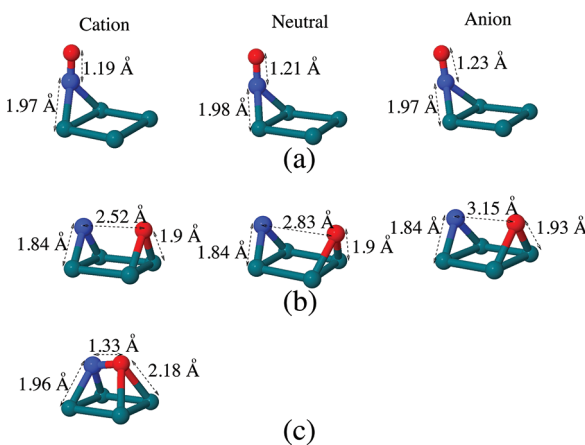


Figure 4. Calculated low-energy atomic configurations for $(\text{Rh}_4 + \text{NO})^\pm$ systems. In (a) and (b) we show results for molecular and dissociative NO adsorption, respectively. In (c) we show our data for the NO molecule attached in a lying-down array. In the left, middle, and right columns we show results for cationic, neutral, and anionic complexes, respectively.

and reverse barriers $\Delta E_b^<$ (leading to the dimerization of N and O atoms) varying from 0.5 to 1.6 eV. The smallest $\Delta E_b^>$ is found for the neutral $\text{Rh}_3 + \text{NO}$ species (Figure 3b) and the largest one for the cationic system (Figure 3a).

Notice that, in the transition state, the N–O bond is broken while both nitrogen and oxygen atoms are bonded to the Rh_3 cluster with equal $R_{\text{Rh}-\text{N}}$ and $R_{\text{Rh}-\text{O}}$ bond lengths of 1.8 Å. Finally, our calculated barriers $\Delta E_b^>$ opposing the breaking of the N–O bond are larger than the ones experimentally obtained on (111) surfaces²⁸ ($\sim 0.67 \pm 0.06$ eV) but are similar to the ones reported by Harding et al.¹⁹ on Rh_6 clusters having triangular units.

We have also calculated the reaction energy paths (not shown) linking Figure 2c-left and c-middle with Figure 2b-left and b-middle, respectively. The existence of the lying-down adsorbed configuration as the initial state of the path lowers the values of $\Delta E_b^>$ to 1.3 and 0.8 eV for positively charged and neutral species, respectively. In the two cases, the breaking of the N–O bond is achieved by a simply stretching mechanism, and this is of course reflected in the notable reduction in the energy barriers. The previous results are in line with the data reported on extended Rh surfaces where the presence of the lying-down adsorbed configuration promotes the easy dissociation of the nitric oxide.

2. $(\text{Rh}_4 + \text{NO})^\pm$ Clusters. In Figure 4 we now show, for different charge states, some low-energy atomic configurations for a NO molecule adsorbed in both molecular (Figure 4a and c) and dissociated (Figure 4b) configurations on the Rh_4 cluster shown in Figure 1b. From our calculations we found that the vertically bonded (on bridge) NO molecule shown in Figure 4a is highly stable. We obtain $R_{\text{Rh}-\text{N}}$ and $R_{\text{N}-\text{O}}$ bond lengths of ~ 2 and 1.2 Å, which are very close to those found in Figure 2 and on extended Rh surfaces. From the dissociated arrays presented in Figure 4b, we observe that N and O atoms are also stable as individual species and that the interatomic distance between them systematically increases, varying as 2.5, 2.8, and 3.1 Å, as we move from cationic, neutral, and anionic clusters, respectively. Finally, from Figure 4c-left we note that the lying-down adsorbed configuration is only stable for the positively charged species, being characterized by a considerably weakened N–O bond (~ 1.33 Å). The previous results clearly illustrate the important role played by the

Table 1. Direct ($\Delta E_b^>$) and Reverse ($\Delta E_b^<$) Energy Barriers (in eV) between the $\text{Rh}_4 + \text{NO}$ Cluster Complexes Shown in Figure 4a and b for Different Charge States

	$(\text{Rh}_4 + \text{NO})^+$	$(\text{Rh}_4 + \text{NO})$	$(\text{Rh}_4 + \text{NO})^-$
$\Delta E_b^>$	1.11	1.23	1.32
$\Delta E_b^<$	0.16	0.47	0.76

ionization state in defining the way NO bonds to a given Rh cluster.

In Table 1, we present our calculated direct $\Delta E_b^>$ and reverse $\Delta E_b^<$ barriers linking Figure 4a-left, a-middle, and a-right with Figure 4b-left, b-middle, and b-right, respectively. Notice that, when compared to Rh_3^\pm , reduced dissociation barriers are required in order to achieve the rupture of the N–O bond, being now almost independent of the ionization state of the clusters and of the order of ~ 1.2 eV. In contrast, the reverse barriers leading to NO formation, $\Delta E_b^<$, are considerably smaller varying from $0.16 \rightarrow 0.47 \rightarrow 0.76$ eV when we move from cationic to neutral to anionic species, respectively.

As in the previous section, we have also calculated the reaction energy path (not shown) linking Figure 4c-left with Figure 4b-left and estimated the values for $\Delta E_b^>$ and $\Delta E_b^<$. Interestingly, we have found a remarkable reduction in the energy barrier required to break the N–O bond, $\Delta E_b^>$ now being of the order of 0.4 eV. We would like to comment that even if the lying-down adsorbed phase is less stable by 0.6 eV when compared with the vertically attached configuration shown in Figure 4a-left, small energy barriers ($\Delta E_b^> \sim 0.4$ eV and $\Delta E_b^< \sim 0.05$ eV) are required to achieve the interconversion between the two types of molecular adsorption.

We compare our calculated data for $\Delta E_b^>$ with the experimental measurements performed on extended Rh(100) surfaces by Villarrubia et al.³² On these square lattices, the lying-down configuration has been found to be stable with an energy barrier opposing the rupture of the N–O bond of $\sim 0.46 \pm 0.03$ eV, which is actually of the order of the one obtained for the $(\text{Rh}_4 + \text{NO})^+$ system discussed in the previous paragraph. We can thus conclude by saying that, for a fixed geometry, modifying the ionization state of Rh_n clusters can considerably alter their adsorption properties and the NO dissociation behavior, revealing the important role played by variations in the electronic structure of the systems. Notice that the lying-down adsorbed phase can become stable or unstable as we move from cationic \rightarrow neutral \rightarrow anionic complexes strongly changing the activation barriers $\Delta E_b^>$ required to break the N–O bond.

3. $(\text{Rh}_6 + \text{NO})^\pm$ Clusters. In this section we present low-energy atomic arrays for a NO species adsorbed in both molecular and dissociated configurations on the six-atom isomers shown in Figure 1c and d. This particular size is interesting to analyze since the experimental findings of Anderson et al.¹⁰ as well as Ford and co-workers¹¹ have revealed a high activity of Rh_6^+ systems toward NO adsorption and dissociation. From Figure 5a we see that, in the octahedral Rh_6^\pm , NO species can be chemisorbed in a vertical manner with $R_{\text{Rh}-\text{N}}$ and $R_{\text{N}-\text{O}}$ bond lengths of ~ 2 and 1.2 Å. These values are the same as the ones found on triangular and square Rh clusters and are also of the order of the ones found by Torres et al.²⁹ addressing NO adsorption on neutral and positively charged Rh_6 clusters. The previous results clearly imply the local character of the $\text{Rh}_n + \text{NO}$ bonding. The dissociated structures shown in Figure 5b are also stable and are defined,

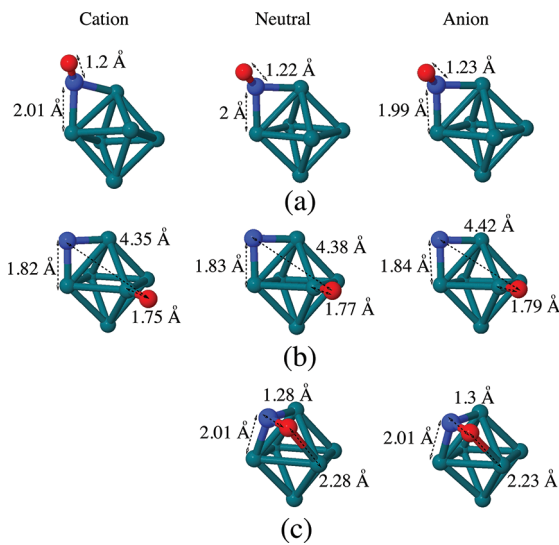


Figure 5. Calculated low-energy atomic configurations for octahedral ($\text{Rh}_6 + \text{NO}$) $^\pm$ systems. In (a) and (b) we show results for molecular and dissociative NO adsorption, respectively. In (c) we show our data for the NO molecule attached in a lying-down array. In the left, middle, and right columns we show results for cationic, neutral, and anionic complexes, respectively.

for all the charge states, by large interatomic separations between the N and O atoms of ~ 4.4 Å. As in Rh_3 , the N atom is attached in an on-bridge configuration while the O species is found in an on-top array. From Figure 5c we observe that the lying-down adsorbed phase only exists for neutral and anionic clusters. Finally we must comment that, for cationic and neutral systems, the vertically attached molecular adsorption is energetically preferred by values of 0.5 and 0.06 eV, respectively, while in the anionic state, the dissociated array (Figure 5b-right) is the most stable atomic configuration.

For Rh_6^+ , it has been experimentally found that, after the NO dissociation reaction, N atoms are highly mobile on the surface of the cluster while oxygen species are found to poison the rhodium structure, leading to the formation of a cluster oxide.¹⁰ In our dissociated configurations shown in Figure 5b, our values for $R_{\text{Rh}-\text{N}}$ and $R_{\text{Rh}-\text{O}}$ are of the same order of magnitude (~ 1.8 Å), and it is thus not easy to establish, from the structural point of view, which atom is more strongly (weakly) bonded to the rhodium structure.

However, interesting trends are obtained when calculating the energy barriers that need to be overcome to achieve single N or O diffusion on the surface of Rh clusters. In Figure 6a and b we plot, as a representative example, the reaction paths obtained when the nitrogen and oxygen atoms adsorbed on the positively charged Rh_6^+ cluster shown in Figure 5b-left perform single lateral displacements as specified in the insets of Figure 6a and b. In a second step, we deduce some relevant energy barriers from these pathways by subtracting well-defined minima and maxima of the energy paths. From Figure 6a we see that the energy barrier opposing the first N-atom displacement is ~ 0.1 eV, while a single lateral movement of the O species shown in Figure 6b requires a barrier of ~ 0.68 eV. These results will be consistent with a higher mobility of the N atom. However, we notice from Figure 6a that subsequent N-atom migration from the center of the triangular unit to the final atomic state (see the inset) requires an energy barrier of ~ 0.54 eV. The previous value is of the order of the ones

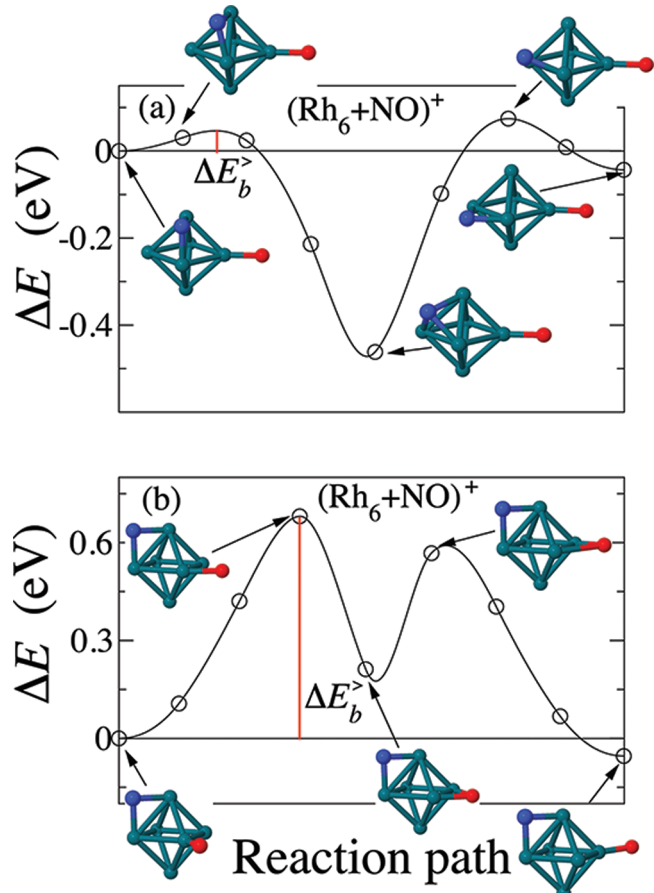


Figure 6. Reaction energy paths obtained for the cationic ($\text{Rh}_6 + \text{N} + \text{O}$) $^+$ system, in which we connect the locally stable initial and final atomic configurations shown as insets in the figures. In (a) [(b)] we show results for the reaction path obtained for a single nitrogen (oxygen) atom displacement. In the figure we specify the height of the direct energy barrier $\Delta E_b^>$ (see text).

Table 2. Direct ($\Delta E_b^>$) and Reverse ($\Delta E_b^<$) Energy Barriers (in eV) between the $\text{Rh}_6 + \text{NO}$ Cluster Complexes shown in Figure 5a and b for Different Charge States (See Text)

	($\text{Rh}_6 + \text{NO}$) $^+$	($\text{Rh}_6 + \text{NO}$)	($\text{Rh}_6 + \text{NO}$) $^-$
$\Delta E_b^>$	1.55	1.26	1.08
$\Delta E_b^<$	1.00	1.20	1.40

found in Figure 6b for different oxygen atom displacements, as well as very close to the diffusion barriers calculated for N and O atoms on Rh(111) surfaces,³⁰ a fact that reveals a complex interplay between atomic diffusion and local atomic environment in these kinds of systems.

In Table 2, we present our calculated direct $\Delta E_b^>$ and reverse $\Delta E_b^<$ barriers linking Figure 5a-left, a-middle, and a-right with Figure 5b-left, b-middle, and b-right, respectively. For all the charge states, high dissociation barriers are required in order to achieve the rupture of the N–O bond, ranging from ~ 1.1 to 1.55 eV. Notice that the reverse barriers vary in the same range of 1–1.4 eV. We have also calculated the reaction energy paths (not shown) linking Figure 5c-middle and c-right with Figure 5b-middle and b-right and estimated the values for $\Delta E_b^>$ and $\Delta E_b^<$. Interestingly,

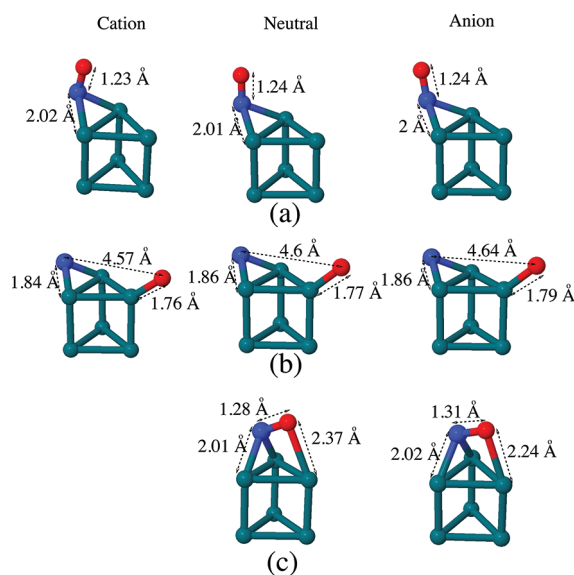


Figure 7. Calculated low-energy atomic configurations for trigonal prism ($\text{Rh}_6 + \text{NO}$) $^\pm$ systems. In (a) and (b) we show results for molecular and dissociative NO adsorption, respectively. In (c) we show our data for the NO molecule attached in a lying-down array. In the left, middle, and right columns we show results for cationic, neutral, and anionic complexes, respectively.

Table 3. Direct ($\Delta E_b^>$) and Reverse ($\Delta E_b^<$) Energy Barriers (in eV) between the $\text{Rh}_6 + \text{NO}$ Cluster Complexes Shown in Figure 7a and b for Different Charge States (See Text)

	$(\text{Rh}_6 + \text{NO})^+$	$(\text{Rh}_6 + \text{NO})$	$(\text{Rh}_6 + \text{NO})^-$
$\Delta E_b^>$	1.83	1.61	1.53
$\Delta E_b^<$	1.25	1.52	1.84

when considering the lying-down adsorbed phase as the initial state of the dissociation path, we found again notable reductions in the energy barriers required to break the N–O bond, $\Delta E_b^>$ now being of the order of ~1 and 0.8 eV for neutral and anionic clusters, respectively.

In Figure 7a and b we present low-energy molecular and dissociated configurations, respectively, for the ($\text{Rh}_6 + \text{NO}$) $^\pm$ system considering the Rh_6 isomer (trigonal prism) shown in Figure 1c. The geometrical characteristics of the NO adsorption are very similar to the ones shown in Figure 5. With respect to the relative stability we must comment that (within our pseudo-potential approach) for cationic and neutral systems, the vertical molecular adsorption is energetically preferred by values of 0.6 and 0.1 eV, respectively, while in the anionic state, the dissociated array (Figure 7b-right) is the most stable atomic configuration. Next, in Table 3, we present our calculated direct $\Delta E_b^>$ and reverse $\Delta E_b^<$ barriers linking Figure 7a-left, a-middle, and a-right with Figure 7b-left, b-middle, and b-right, respectively. Note that (i) NO dissociation (as in previous cases) on the triangular unit involves high-energy barriers ($\Delta E_b^>$) that vary in the range of 1.5–2 eV and that (ii) the reverse barriers $\Delta E_b^<$ are of the same order of magnitude. As a systematic trend we also found that the reaction energy paths (not shown) linking Figure 7c-middle and c-right with Figure 7b-middle and b-right yield values for $\Delta E_b^>$ which are reduced to 1.4 and 1 eV for neutral and anionic species, respectively. Even if the previous

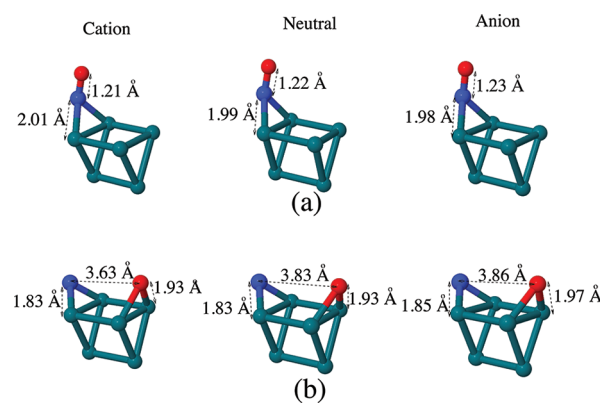


Figure 8. Calculated low-energy atomic configurations for trigonal prism ($\text{Rh}_6 + \text{NO}$) $^\pm$ systems. In (a) and (b) we show results for molecular and dissociative NO adsorption, respectively. In the left, middle, and right columns we show results for cationic, neutral, and anionic complexes, respectively.

Table 4. Direct ($\Delta E_b^>$) and Reverse ($\Delta E_b^<$) Energy Barriers (in eV) between the $\text{Rh}_6 + \text{NO}$ Cluster Complexes Shown in Figure 8a and b for Different Charge States (See Text)

	$(\text{Rh}_6 + \text{NO})^+$	$(\text{Rh}_6 + \text{NO})$	$(\text{Rh}_6 + \text{NO})^-$
$\Delta E_b^>$	1.26	1.11	1.02
$\Delta E_b^<$	0.40	0.65	0.81

energy barriers are still high, it is clear that the existence of the lying-down adsorbed configuration promotes an easier dissociation of the nitric oxide.

Similar to Figure 7a, in Figure 8a we present low-energy atomic arrays for a single NO molecule vertically adsorbed in an on-bridge configuration, but, in contrast to Figure 7a, the terminal O atom is oriented toward one of the square units of the structure. In Figure 8b we show the equilibrium configurations for some dissociated arrays with different charge states. The analysis of reaction paths linking Figure 8a-left, a-middle, and a-right with Figure 8b-left, b-middle, and b-right, respectively, implies that the NO dissociation will occur now on the square unit of the trigonal prism. This calculation is interesting to perform to evaluate the role of the local atomic environment on the dissociation of the nitric oxide. In Table 4 we show our calculated direct $\Delta E_b^>$ and reverse $\Delta E_b^<$ barriers. When compared with the data shown in Table 3, we see that NO decomposition is easier to obtain on the square units of the cluster. In addition, as shown in Table 1 for the Rh_6^\pm clusters, we observe that the energy barriers required to break the N–O bond are very similar and vary between 1.26 and 1.02 eV, being almost independent of the charge state of the systems. Interestingly, the lying-down chemisorbed configuration was unstable for all the charge states.

With respect to the relative stability, we obtain that the adsorption of a single NO molecule perturbs the energy differences between the two considered six-atom isomers shown in Figure 1. In fact, the lowest energy atomic array for cationic and neutral species corresponds now, by values of ~0.1 eV, to the structures shown in Figure 8a-left and a-middle, being defined by a trigonal prism with a NO molecule vertically attached in an on-bridge configuration. However, in the anionic state, the dissociated structure shown in Figure 5b-right is the preferred array

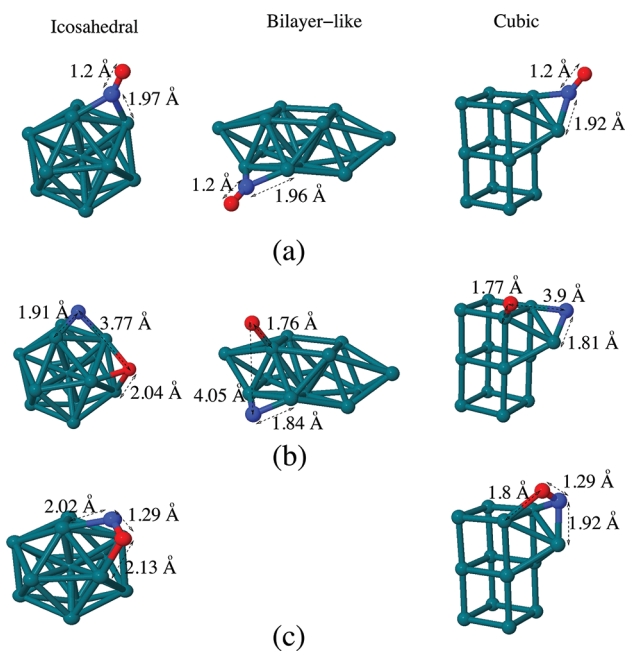


Figure 9. Calculated low-energy atomic configurations for $(\text{Rh}_{13} + \text{NO})^+$ clusters. In (a) and (b) we show results for molecular and dissociative NO adsorption, respectively. In (c) we show our data for the NO molecule attached in a lying-down array. In the left, middle, and right columns we show results for icosahedral, bilayer-like, and cubic Rh clusters, respectively.

(by values as large as 0.6 eV), a relative stability that is maintained even if we perform a full optimization of the systems.

We can thus conclude this section by saying that in the experiments of Anderson et al.¹⁰ as well as Ford and co-workers,¹¹ the gas phase $(\text{Rh}_n + \text{NO})^\pm$ species are identified on the basis of their mass alone, and no direct information is obtained regarding the structure of the Rh_n clusters. Our calculations have revealed the high affinity observed for Rh_6 clusters toward NO attachment (in both molecular and dissociated forms), having adsorption energies that are in the range of 2–2.5 eV in good agreement with previous theoretical calculations.²⁹ In addition, our theoretical data have underlined the importance of the geometrical structure and charge state in determining the reactivity of Rh_n clusters. Finally, we found that the existence of a lying-down adsorbed configuration for the NO species leads to the formation of $(\text{Rh}_6 + \text{NO})^\pm$ cluster complexes with a highly activated N–O bond as well as reduced values for $\Delta E_b^>$, and an adsorbed phase could be at the origin of the measured data.

4. $(\text{Rh}_{13} + \text{NO})^+$ Clusters. For 13-atom clusters, the reported experimental data addresses only the catalytic activity of positively charged Rh_{13}^+ species. For this number of Rh atoms, no evidence of N_2 production is observed and only a simple sequential molecular adsorption dominates the surface chemistry,¹⁰ a fact that will be consistent with the existence of high-energy barriers opposing the N–O bond breakage. Due to the low symmetry of the bilayer-like and cubic 13-atom clusters shown in Figure 1f and g, respectively, there is a large number of possible chemisorption sites available for the NO molecule on the surface of the particles. In these cases, we did not carry out a complete search to find the global minimum. Instead, we simply started from contrasting initial atomic arrays and performed (as in previous cases) a constrained geometry optimization procedure. We

Table 5. Direct ($\Delta E_b^>$) and Reverse ($\Delta E_b^<$) Energy Barriers (in eV) between the $\text{Rh}_{13} + \text{NO}$ Cluster Complexes Shown in Figure 9a and b for Different Charge States (See Text)

	$(\text{Rh}_{13} + \text{NO})^+$ icosahedral	$(\text{Rh}_{13} + \text{NO})^+$ bilayer-like	$(\text{Rh}_{13} + \text{NO})^+$ cubic
$\Delta E_b^>$	1.45	2.00	1.56
$\Delta E_b^<$	1.93	1.12	0.64

considered a total of 10 different vertically adsorbed molecular configurations for each cluster, and in Figure 9a, we show our lowest energy atomic structures. From Figure 9a and b we notice that the vertical NO adsorption and the individually attached N + O species, respectively, are stable in all Rh_{13}^+ structures. In addition, we see from Figure 9c that the lying-down chemisorbed configuration around the adsorption sites shown in Figure 9a is only stable for the icosahedral (Figure 9c-left) and cubic (Figure 9c-right) structures, being defined by elongated N–O bonds of the order of 1.29 Å. As in previous cases, the lying-down adsorption is found to be less stable by ~ 0.2 –0.3 eV with respect to the vertically attached NO species, but, as already stated, small interconversion energy barriers of ~ 0.4 eV are obtained between the two types of molecular adsorption.

In Table 5, we present our calculated direct $\Delta E_b^>$ and reverse $\Delta E_b^<$ barriers linking Figure 9a-left, a-middle, and a-right with Figure 9b-left, b-middle, and b-right, respectively. As in previous cases high dissociation barriers are required in order to achieve the rupture of the N–O bond, ranging from ~ 1.45 to 2.0 eV. We have also calculated the reaction energy paths (not shown) linking Figure 9c-left and c-right with Figure b-left and b-right and estimated the values for $\Delta E_b^>$ and $\Delta E_b^<$. When considering the lying-down adsorbed phase as the initial state of the dissociation path, we obtain notable reductions in the energy barriers required to break the N–O bond, $\Delta E_b^>$ now being of the order of ~ 1 eV.

From the previous data it is clear that the breaking of the N–O bond on our here-considered Rh_{13}^+ structures will be very difficult to realize. Notice that the here-obtained cluster reactivity is determined by a complex interplay between the local atomic environment and electronic effects. On the one hand, the abundance of square and triangular units for a given cluster structure will play a fundamental role in determining their adsorption properties and catalytic activity, but, on the other hand, altered electronic structures (different charge states) can stabilize various types of adsorbed configurations (lying-down, vertically attached, etc.) for the NO species strongly changing also the dissociation behavior.

In fact, in the work of Anderson et al.¹⁰ it has been found that for Rh_{13}^+ it is possible to saturate the cluster surface with a maximum of 12 NO molecules yielding the $[\text{Rh}_{13}(\text{NO})_{12}]^+$ compound. Consequently, we have done additional calculations by fully saturating the surface of our considered Rh_{13}^+ isomers and performing a global optimization of the systems. From our data (not shown) we have obtained that the icosahedral structure, being the only one to support a nonsurface atom, can adsorb a maximum of 12 NO species with an adsorption energy of ~ 2.8 eV. In addition, the surface of this cluster is defined only by triangular units (see Figure 1e) which (as has been demonstrated in the previous sections) is a local atomic environment characterized by high NO dissociation energy barriers, making thus this 13-atom structure a catalytically inert cluster. The previous data could explain the

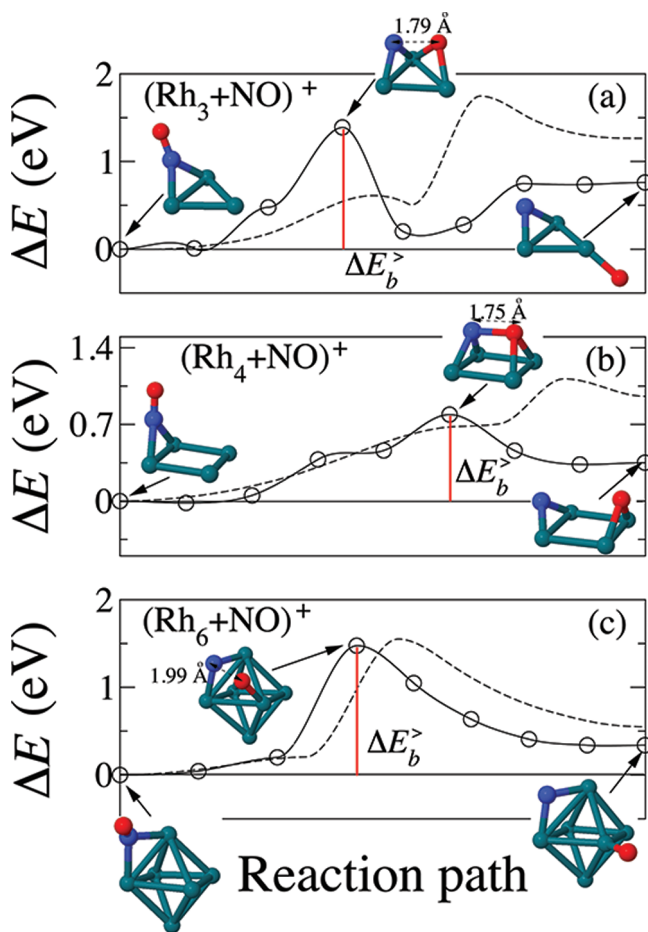


Figure 10. Reaction energy paths connecting a molecularly adsorbed NO species with a dissociated array of N and O atoms, as shown as insets in the figures, assuming fully relaxed initial and final atomic configurations. In (a), (b), and (c) we show results for $(\text{Rh}_3 + \text{NO})^+$, $(\text{Rh}_4 + \text{NO})^+$, and $(\text{Rh}_6 + \text{NO})^+$ systems, respectively. In the figure we also specify the values of the N–O interatomic separation at the transition state as well as the height of the direct dissociation energy barrier $\Delta E_b^>$ (see text). For comparison, the results of frozen-cluster calculations are also included as a dashed line.

absence of N–O bond breaking in the samples and could also imply that the presence of high-energy isomers might be responsible for the observed catalytic behavior.

5. Role of Cluster Relaxation. Clearly, our controlled calculations on frozen Rh clusters have been of fundamental importance in order to isolate the specific contributions of N and O atoms on the dissociation behavior of nitric oxide. However, upon NO adsorption and dissociation, structural perturbations in our Rh_n clusters are expected to occur. We have thus recalculated the reaction energy paths of our here-considered cationic $(\text{Rh}_n + \text{NO})^+$ clusters by fully relaxing all the atoms of the structures. In Figure 10 we show, as representative examples, our data for $(\text{Rh}_3 + \text{NO})^+$, $(\text{Rh}_4 + \text{NO})^+$, and $(\text{Rh}_6 + \text{NO})^+$ systems. From the insets of Figure 10 we note, when comparing with Figures 2, 3, 4, and 5, appreciable global atomic rearrangements on the initial and final states, as well as during the rupture of the N–O bond, the previous variations being as expected more notable for the (smallest) Rh_3^+ and Rh_4^+ systems. In addition, when comparing with the frozen-cluster calculations (dashed lines), we observe that the reaction energy paths are strongly affected by the reconstruction

of the Rh cluster atoms (in particular for the Rh_3^+ cluster), leading in general to the formation of smaller values for $\Delta E_b^>$.

Notice that, in the case of the octahedral Rh_6^+ structure (Figure 10c), including relaxation effects of the Rh cluster atoms induces in general small changes in the atomic positions and on the reaction energy paths (only a rigid shift of the energy maxima is found). The height of the NO dissociation barrier is practically the same, being still larger than 1 eV. Similar results are found for the Rh_6^+ trigonal prism as well as for the 13-atom clusters (not shown), where the full relaxation leaves the reaction paths nearly unperturbed. The previous data clearly define the local character of the NO bonding and validate, for larger sizes, our restricted optimization approach.

IV. SUMMARY AND CONCLUSIONS

In this work, we have presented an extensive pseudopotential density functional theory study dedicated to analyze the stability and dissociation behavior of NO molecules adsorbed on small nonmagnetic Rh_n^\pm clusters. We have considered Rh_n structures of different sizes ($n = 3, 4, 6$, and 13) and charge states on which NO species have been adsorbed in both molecular and dissociative configurations. We obtain that the relative stability between different bare Rh_n^\pm isomers depends on the ionization state of the clusters as well as on the presence of adsorbed NO species on their surface. Furthermore, various adsorbed configurations for the nitric oxide molecules are found when switching from cationic to neutral to anionic clusters. The nudged elastic band method reveals that the dissociation of the N–O bond is more easily obtained on square facets than on triangular atomic environments, a fact that indirectly provides some structural features of the Rh_n^\pm clusters present in the gas phase experiments. The energy barriers that need to be overcome to achieve the breaking of the N–O bond strongly depend on the charge state and size of the systems (ranging from 0.4 to 2.0 eV), a fact that could be used to accurately tune the catalytic activity of these types of materials. Finally, we would like to conclude by emphasizing that (i) high-energy isomers could be responsible, at some stage, for the experimentally observed reactivity of Rh_n^\pm systems, as well as to (ii) underline the possibility that more subtle effects related to the coadsorption of additional NO species could play an important role in the dissociation behavior. Calculations along this line of research are currently underway.

AUTHOR INFORMATION

Corresponding Author

*E-mail: guirado@ifisica.uaslp.mx

ACKNOWLEDGMENT

R.A.G.-L. acknowledges the financial support from PROMEP (SEP-México) and CONACyT (México) through grants CA230 and 169345, respectively. Computer resources from the Centro Nacional de Supercomputación (CNS) of the Instituto Potosino de Investigación Científica y Tecnológica (IPICyT), SLP, México, are also acknowledged.

REFERENCES

- Sun, S.; Murray, C. B.; Weller, D.; Folks, L.; Moser, A. *Science* **2000**, 287, 1989.
- Chung, S. H.; Hoffmann, A.; Guslienko, K.; Bader, S. D.; Liu, C.; Kay, B.; Makowski, L.; Chen, L. *J. Appl. Phys.* **2005**, 97, 10R101.

- (3) Nam, J. W.; Thaxton, C. S.; Mirkin, C. A. *Science* **2003**, *301*, 1884.
- (4) Tsang, S. C.; Yu, C. H.; Gao, X.; Tam, K. *J. Phys. Chem. B* **2006**, *110*, 16914.
- (5) Burgel, C.; Reilly, N. M.; Johnson, G. E.; Mitric, R.; Kimble, M. L.; Castleman, A. W.; Bonacic-Koutecky, V. *J. Am. Chem. Soc.* **2008**, *130*, 1694.
- (6) Hanamura, T.; Ichihashi, M.; Watanabe, Y.; Isomura, N.; Kondow, T. *J. Phys. Chem. A* **2007**, *111*, 422.
- (7) Swart, I.; Fielicke, A.; Redlich, B.; Meijer, G.; Weckhuysen, B. M.; de Groot, F. M. F. *J. Am. Chem. Soc.* **2007**, *129*, 2516.
- (8) Wen, X. D.; Li, Y. W.; Wang, J.; Jiao, H. *J. Phys. Chem. B* **2006**, *110*, 21060.
- (9) Datta, S.; Kabir, M.; Saha-Dasgupta, T.; Mookerjee, A. *Phys. Rev. B* **2009**, *80*, 085418.
- (10) Anderson, M. L.; Ford, M. S.; Derrick, P. J.; Drewello, T.; Woodruff, D. P.; Mackenzie, S. R. *J. Phys. Chem. A* **2006**, *110*, 10992.
- (11) Ford, M. S.; Anderson, M. L.; Barrow, M. P.; Woodruff, D. P.; Drewello, T.; Derrick, P. J.; Mackenzie, S. R. *Phys. Chem. Chem. Phys.* **2005**, *7*, 975.
- (12) Loffreda, D.; Simon, D.; Sauset, P. *J. Chem. Phys.* **1998**, *108*, 6447.
- (13) Rempel, J.; Greeley, J.; Hansen, L. B.; Nielsen, O. H.; Norskov, J. K.; Mavrikakis, M. *J. Phys. Chem. C* **2009**, *113*, 20623.
- (14) Tang, H.; Trout, B. L. *J. Phys. Chem. B* **2005**, *109*, 17630.
- (15) Inderwildi, O. R.; Lebiedz, D.; Deutschmann, O.; Warnatz, J. *J. Chem. Phys.* **2005**, *122*, 154702.
- (16) Nolte, P.; Stierle, A.; Jin-Phillipp, N. Y.; Kasper, N.; Schulli, T. U.; Dosch, H. *Science* **2008**, *321*, 1654.
- (17) Grass, M. E.; Zhang, Y.; Butcher, D. R.; Park, J. Y.; Li, Y.; Bluhm, H.; Bratlie, K. M.; Zhang, T.; Somorjai, G. A. *Angew. Chem., Int. Ed.* **2008**, *47*, 8893.
- (18) Park, J. Y.; Zhang, Y.; Grass, M.; Zhang, T.; Somorjai, G. A. *Nano Lett.* **2008**, *8*, 673.
- (19) Harding, D.; Mackenzie, S. R.; Walsh, T. R. *J. Phys. Chem. B* **2006**, *110*, 18272.
- (20) Henkelman, G.; Uberuaga, B. P.; Jonsson, H. *J. Chem. Phys.* **2000**, *113*, 9901.
- (21) Baroni, S.; Dal Corso, A.; de Gironcoli, S.; Giannozzi, P.; Cavazzoni, C.; Ballabio, G.; Scandolo, S.; Chiarotti, G.; Focher, P.; Pasquarello, A.; Laasonen, K.; Trave, A.; Car, R.; Marzani, N.; Kokalj, A. <http://www.pwscf.org/>.
- (22) Perdew, J. P.; Burke, K.; Ernzerhof, M. *Phys. Rev. Lett.* **1996**, *77*, 3865.
- (23) Harding, D. J.; Walsh, T. R.; Hamilton, S. M.; Hopkins, W. S.; Mackenzie, S. R.; Gruene, P.; Haertelt, M.; Meijer, G.; Fielicke, A. *J. Chem. Phys.* **2010**, *132*, 011101. Harding, D. J.; Gruene, P.; Haertelt, M.; Meijer, G.; Fielicke, A.; Hamilton, S. M.; Hopkins, W. S.; Mackenzie, S. R.; Neville, S. P.; Walsh, T. R. *J. Chem. Phys.* **2010**, *133*, 214304.
- (24) Chou, J. P.; Chen, H. Y. T.; Hsing, C. R.; Chang, C. M.; Cheng, C.; Wei, C. M. *Phys. Rev. B* **2009**, *80*, 165412.
- (25) Chang, C. M.; Chou, M. Y. *Phys. Rev. Lett.* **2004**, *93*, 133401.
- (26) Bae, Y. C.; Kumar, V.; Osanai, H.; Kawazoe, Y. *Phys. Rev. B* **2005**, *72*, 125427.
- (27) Fukui, K. *Acc. Chem. Res.* **1971**, *4*, 57.
- (28) Borg, H. J.; Reijerse, J. F. C. M.; van Santen, R. A.; Niemantsverdriet, J. W. *J. Chem. Phys.* **1994**, *101*, 10052.
- (29) Torres, M. B.; Aguilera-Granja, F.; Balbás, L. C.; Vega, A. *J. Phys. Chem. A* **2011**, *115*, 8350.
- (30) Mavrikakis, M.; Rempel, J.; Greeley, J.; Hansen, L. B.; Norskov, J. K. *J. Chem. Phys.* **2002**, *117*, 6737.
- (31) Knickelbein, M. *Chem. Phys. Lett.* **2002**, *353*, 221.
- (32) Villarrubia, J. S.; Ho, W. *J. Chem. Phys.* **1987**, *87*, 750.
- (33) Xiao, L.; Wang, L. *J. Phys. Chem. A* **2004**, *108*, 8605.
- (34) Dong, C. D.; Xong, X. G. *Phys. Rev. B* **2008**, *78*, 020409.
- (35) Sessi, V.; Kuhnke, K.; Zhang, J.; Honolka, J.; Kern, K.; Tieg, C.; Sipr, O.; Minar, J.; Ebert, H. *Phys. Rev. B* **2010**, *82*, 184413.